Modulation of Fibrillogenesis of Amyloid β(1−40) Peptide with Cationic Gemini Surfactant

Meiwen Cao, Yuchun Han, Jinben Wang, and Yilin Wang*

Key Laboratory of Colloid and Interface Science, Institute of Chemistry, Chinese Academy of Sciences, Beijing 100080, P. R. China

Received: July 6, 2007; In Final Form: September 17, 2007

Modulation of the fibrillogenesis of amyloid peptide Aβ(1−40) with the cationic gemini surfactant hexamethylene-1,6-bis(dodecyldimethylammonium bromide) ($C_{12}C_6C_{12}Br_2$) has been studied. Both UV−vis and AFM results show that $C_{12}C_6C_{12}Br_2$ monomers can promote the fibrillogenesis of Aβ(1−40) while its micelles inhibit this process. The electrostatic/hydrophobic force balance plays important roles in determining the Aβ(1−40) aggregation style and the secondary structures. When the surfactant positive charges are close to the Aβ(1−40) negative charges in number, the hydrophobic interaction is highly enhanced in the system. Both the nucleation rate and the lateral association between fibrils are greatly promoted. However, when the surfactant positive charges are in excess of the Aβ(1−40) negative charges, the electrostatic interaction is strengthened. In this case, the lateral association is inhibited and the α-helix to β-sheet transition in the secondary structure is prevented. Simultaneously, another assembly pathway is induced to give the amorphous aggregates. Moreover, the size and surface roughness of the Aβ(1−40) aggregates also vary upon increasing $C_{12}C_6C_{12}Br_2$ concentration.

Introduction

Alzheimer's disease (AD)[1] is one of the so-called "conformational diseases" in which proteins may misfold into amyloid aggregates. Brains of AD patients contain a large amount of extracellular amyloid deposits with amyloid β-peptide (Aβ) that is generated from cleavage of a larger amyloid precursor protein (APP).[2,3] The most abundant forms of the cleaved peptides are 40 (∼90%) and 42 (∼10%) amino acids. Amyloid fibrillogenesis is a very complex process that can be affected by various extrinsic or environmental factors such as pH, peptide concentration, solvent hydrophobicity, temperature, ionic strength, metal ions, and so on.[4−6] The fibrillogenesis involves the secondary structure transition from disordered random structure to ordered β-sheet conformation.[7] The formed fibrils have a general cross-β structure consisting of successive hydrogen-bonded β-strands lying perpendicular to the fibril axis.[8]

Amyloid fibrillogenesis is a multistep process where the peptide can aggregate into multiple amyloid aggregates, such as oligomers, protofibrils, and fibrils.[9−12] These different aggregates have different underlying molecular conformations and significantly different toxicities in neuronal cell cultures.[10,12−14] The mature amyloid fibril was previously thought to be the only toxic species of Aβ peptide.[14] Recently, soluble Aβ oligomers and protofibrils have been proved to possess more neural toxicity than both monomers and insoluble mature fibrils due to their membrane pore-forming capabilities.[2,15,16] Moreover, even at the same assembly stage, for example, fibrils, they commonly exhibit different neurotoxicities with multiple distinct morphologies.[10,11,13] For example, Petkova et al.[10] have shown that the toxicity of quiescent fibrils is significantly higher than that of agitated fibrils. Lührs et al.[12] have found that more ordered and longer fibrils are more toxic. On the basis of this knowledge, various different strategies have been proposed for AD therapy. An attractive therapeutic approach is to reduce the levels of the toxic oligomers.[16,17] Another choice is to transform toxic low-molecular-weight oligomers into high-molecular-weight aggregates with lower toxicity.[17,18]

Various reagents have been developed to modulate the fibrillogenesis of Aβ peptide.[19] Among these reagents, surfactants are one important category. Pertinhez et al.[20] and Shao et al.[21] have demonstrated that, in the presence of sodium dodecyl sulfate (SDS) micelles, Aβ(1−40) remains monomeric and an α-helix state while resting upon the periphery of the SDS micelle. This conformation disables amyloid fibril formation. Wood et al.[22] have compared the effect of several surfactants on the aggregation of Aβ peptide and found selective inhibition of Aβ fibril formation by hexadecyl-*N*-methylpiperidinium (HMP) bromide. Sabaté et al.[23,24] and Wang et al.[25] have demonstrated the concentration-dependent manner of the inhibition of Aβ fibril formation with surfactants. Very recently, we reported the interaction of Aβ(1−40) with a cationic gemini surfactant hexamethylene-1,6-bis(dodecyldimethylammonium bromide) [$C_{12}H_{25}(CH_3)_2N(CH_2)_6N(CH_3)_2C_{12}H_{25}]Br_2$ ($C_{12}C_6C_{12}Br_2$).[26] We mainly focused on the thermodynamics of the Aβ(1−40)−surfactant interaction as well as the different effect of single-chain surfactant and gemini surfactant on Aβ fibrillogenesis within a short time limit. Compared with the single-chain surfactant DTAB, $C_{12}C_6C_{12}Br_2$ has a much stronger binding ability with Aβ(1−40) so that induces its fibril formation at a very low surfactant concentration. However, much remains to be elucidated regarding the effect of the surfactant concentration on the dynamic of Aβ fibrillogenesis, and the morphologies, sizes, and the secondary structures of Aβ aggregates with time.

In this article, the dynamic of Aβ(1−40) fibrillogenesis and the variation of the morphological and structural characteristics of Aβ(1−40) aggregates at different $C_{12}C_6C_{12}Br_2$ concentrations have been investigated systematically. The results indicate that $C_{12}C_6C_{12}Br_2$ can regulate β-amyloid aggregation. It can not only promote (by monomers) or inhibit (by micelles) the fibril

* Author to whom correspondence should be addressed. E-mail: yilinwang@iccas.ac.cn.

10.1021/jp075271b CCC: $37.00
Published on Web 11/06/2007

formation, but also induce an alternate assembly pathway to form amorphous aggregates. The polymorphism is found to be a predominant characteristic in amyloid fibrils, which is possibly caused by the lateral association between fibrils. Addition of $C_{12}C_6C_{12}Br_2$ can significantly change the lateral association in a concentration-dependent manner. Binding of $C_{12}C_6C_{12}Br_2$ molecules with A$\beta(1-40)$ affects the morphology and surface roughness of the aggregates. Moreover, a higher concentration of $C_{12}C_6C_{12}Br_2$ monomers and $C_{12}C_6C_{12}Br_2$ micelles can prevent the α-helix to β-sheet transformation of the A$\beta(1-40)$ secondary structure. These findings may be helpful in guiding the development and design of an effective reagent to control the aggregation of A$\beta(1-40)$ for AD therapy.

Experimental Section

Materials. The peptide used was fragment 1−40 of Aβ (trifluoroacetate salt) obtained from GL Biochem (Shanghai) Ltd. (A$\beta(1-40)$, Lot No. GLS-2006-11-02-Q07). The purity of the peptide was greater than 96%. Gemini surfactant $C_{12}C_6C_{12}Br_2$ was synthesized and purified according to the method of Menger and Littau.[27] The structure of $C_{12}C_6C_{12}Br_2$ was confirmed by ^{1}H NMR spectroscopy, and the purity was verified by elemental analysis and surface tension measurements. 1,1,1,3,3,3-Hexafluoro-2-propanol (HFIP) was from ACROS. Pure water (18 MΩ cm^{-1}) was obtained from the Milli-Q system and used in all experiments.

Aβ(1−40) Preparation. In order to prepare the reliable and reproducible β-amyloid stock solutions, possible contamination by bacteria was addressed by autoclaving all pipet tips, vials, and buffer solutions. The removal of dust from the buffered solutions was accomplished by filtering with non-rinsed inorganic Anotop 0.02-μm filters. A$\beta(1-40)$ in nonaggregated form was prepared as described previously.[28] Briefly, a stock solution was prepared by dissolving ∼0.72 mg of A$\beta(1-40)$ in 800 μL of HFIP, which was incubated at room temperature for 1 h in sealed vials. Then, the solution was bath-sonicated for 30 min until A$\beta(1-40)$ dissolved completely. After that, the solution was kept at 4 °C for 30 min to avoid solvent evaporation when aliquoting. Once the sample was aliquoted, HFIP was removed from the disaggregated peptide by evaporation under a gentle stream of nitrogen, leaving a slightly yellow film. Just before initiating the following experiments, an aliquot of A$\beta(1-40)$ was dissolved in 1.0 mL of $C_{12}C_6C_{12}Br_2$ solutions of different concentrations at Tris-HCl buffer concentration of 10 mM (pH 7.4). The molecular weight of A$\beta(1-40)$ is about 4.3 kD, and the final peptide molar concentration is ∼42 μM. The prepared solutions were then kept at 26 ± 1 °C for the following experiments.

Turbidity Measurements. Turbidity measurements were carried out with a Hitachi U-3010 PC UV/vis spectrophotometer. The turbidity of the peptide solutions in the absence or presence of $C_{12}C_6C_{12}Br_2$ at different concentrations was monitored by UV absorbance at 400 nm at 2-h or 1-day intervals. A cuvette with a 1-cm pathway was used.

Circular Dichroism (CD). CD spectra were recorded on a JASCO J-815 spectrophotometer at room temperature using a 2.0-mm quartz cell. Scans were obtained in a range between 190 and 260 nm by taking points at 0.2 nm, with an integration time of 0.5 s. Typically, five spectra were averaged to improve the signal-to-noise ratio. The spectra were smoothed using the noise-reducing option in the software supplied by the vendor. The results were represented as molar residue ellipticity (theta, in units of kdeg cm^2 dmol^{-1}), taking a value of 108 as the mean residue weight for the A$\beta(1-40)$ peptide. Deconvolution calculations of the CD spectra were performed to obtain the percentages of each secondary structure using the online CD analysis program (K2D DICHROWEB http://www.cryst.bbk.ac.uk/ cdweb/html/home.html).[29]

Atomic Force Microscopy (AFM). A Multimode Nanoscope IIIa AFM (Digital Instruments, CA) was used for AFM imaging. For ambient imaging, 5−10 μL of A$\beta(1-40)$ sample solution was deposited onto a freshly cleaved piece of mica and left to adhere for 5−10 min. The sample was then briefly rinsed with 100 μL of Milli-Q water and dried with a gentle stream of nitrogen. Probes used were etched silicon probes attached to 125-μm cantilevers with a nominal spring constant of 40 N/m (Digital Instruments, model RTESPW). Tapping mode images were obtained with a scan speed of 1.0−1.8 Hz, a tip resonance frequency of 230−300 kHz, and a drive amplitude of 20−100 mV. Height and amplitude data were simultaneously collected as 512 × 512 pixel images. Topographic data were regularly recorded in both trace and retrace to check on scan artifacts. Analysis of the images was carried out using the Digital Instruments Nanoscope software (version 512r2).

Transmission Electron Microscopy (TEM). TEM samples were prepared from the peptide solutions using a negative-staining method, and 1% uranyl acetate solution was used as the staining agent. A drop of the solution was placed onto a carbon Formvar-coated copper grid, and the excess liquid was sucked away by filter paper. After drying, the samples were imaged under electron microscope (JEOL 2010).

Results and Discussion

Our recent study[26] has shown that cationic gemini surfactant $C_{12}C_6C_{12}Br_2$ can induce the early stage aggregation of A$\beta(1-40)$ in a concentration-dependent fashion. Three regions that are dominated by different interactions between A$\beta(1-40)$ and $C_{12}C_6C_{12}Br_2$ are observed. In region I, $C_{12}C_6C_{12}Br_2$ concentration is below its critical micelle concentration (cmc) and the number of positive charges on $C_{12}C_6C_{12}Br_2$ is less than the number of negative charges on A$\beta(1-40)$. The surfactant monomers electrostatically bind on A$\beta(1-40)$, which facilitates the conformational transition from random structure to ordered β-sheet structure. In region II, $C_{12}C_6C_{12}Br_2$ concentration is still below the cmc; however, the surfactant positive charges are in excess of the Aβ negative charges. In this case, the ordered β-sheet structure starts to be disrupted due to the repulsive interaction among the head groups of $C_{12}C_6C_{12}Br_2$ bound on A$\beta(1-40)$ as well as the formation of small hydrophobic clusters by the surfactant molecules. Then, in region III where the $C_{12}C_6C_{12}Br_2$ concentration is above the cmc, the globular aggregates of A$\beta(1-40)$ molecules are induced by the micelles mainly through the hydrophobic interaction between the surfactant hydrocarbon chains and hydrophobic residues of Aβ-(1−40).

In the present study, the concentration of A$\beta(1-40)$ is fixed at 42 μM, while three $C_{12}C_6C_{12}Br_2$ concentrations are chosen at 0.05, 0.3, and 2.5 mM, which lie in the interaction regions of I, II, and III, respectively. The effect of surfactant concentration on the A$\beta(1-40)$ fibrillogenesis rate, the assembly pathways, the aggregate morphologies and sizes, and the secondary structures have been investigated. The A$\beta(1-40)$ fibrillogenesis in the absence of $C_{12}C_6C_{12}Br_2$ is also studied for comparison.

Effect of Gemini Surfactant Concentration on Fibrillogenesis Rate of Aβ(1−40). We first determine the fibrillogenesis rate of A$\beta(1-40)$ at different surfactant concentrations using turbidity measurements. The results are shown in Figure 1. In the turbidity curves with a typical sigmoidal profile, the small-

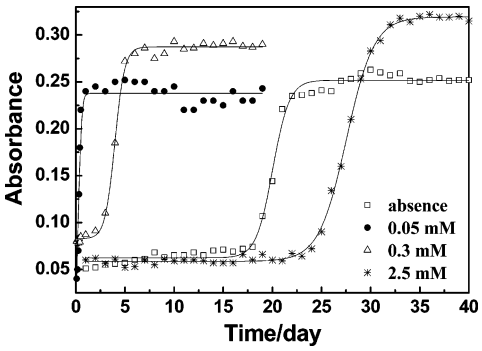

Figure 1. Turbidity results showing the dependence of the fibrillogenesis of Aβ(1−40) on time in the absence of $C_{12}C_6C_{12}Br_2$ or in the presence of 0.05, 0.3, and 2.5 mM $C_{12}C_6C_{12}Br_2$.

TABLE 1: Time Courses for Aβ(1−40) To Produce Protofibrils and Mature Fibrils at Different $C_{12}C_6C_{12}Br_2$ Concentrations Obtained from AFM Results

	0 mM	0.05 mM	0.3 mM	2.5 mM
protofibrils	∼18 d	4−6 h	∼3 d	∼21 d
fibrils	∼24 d	∼1 d	∼8 d	∼28 d

to-large change of turbidity values indicates the evolution of aggregates from nonfibrillar forms with smaller sizes to fibrillar forms with larger sizes.[23] Differences in the lag time indicate that the surfactant concentration can dramatically affect the fibrillogenesis of Aβ(1−40), and the rate of Aβ fibrillogenesis at different $C_{12}C_6C_{12}Br_2$ concentrations is in the order of 0.05 mM > 0.3 mM > 0 mM > 2.5 mM. In the absence of $C_{12}C_6C_{12}Br_2$, Aβ(1−40) itself needs ∼22 days to finish the fibrillogenesis, similar to the result by Harper et al.[30] However, the time course of fibrillogenesis is shortened to ∼1 and ∼6 days by adding 0.05 and 0.3 mM $C_{12}C_6C_{12}Br_2$, respectively, while it is elongated to ∼31 days by 2.5 mM $C_{12}C_6C_{12}Br_2$. Since the cmc of $C_{12}C_6C_{12}Br_2$ is about 1.0 mM,[31] we can conclude that the surfactant monomers act as promoters of fibril formation and shorten the lag time, while the surfactant micelles inhibit the aggregation kinetically. Moreover, for the sections in UV−vis curves corresponding to the transition of aggregates from nonfibrillar to fibrillar form, the sharpness is more pronounced at lower surfactant concentrations than at higher ones. This implies whether or not the surfactant shortening or elongating of the rate of the Aβ(1−40) fibrillogenesis depends on the surfactant concentration. These stimulatory and inhibitory effects of $C_{12}C_6C_{12}Br_2$ on Aβ(1−40) fibrillogenesis are similar to the results reported by Sabaté et al., who studied the effect of cationic single-chain surfactant DTAB, TTAB, and CTAB.[23]

We also use AFM to confirm the fibrillogenesis of Aβ(1−40) at different $C_{12}C_6C_{12}Br_2$ concentrations. The typical fibrillogenesis process of Aβ peptide, which involves different assembly stages in the order of oligomers, protofibrils, and mature fibrils with the elapse of time, are observed in all the cases (see Supporting Information). However, the time needed to reach the same assembly stage is apparently different. We summarize the time courses for Aβ(1−40) to produce protofibrils and mature fibrils at different $C_{12}C_6C_{12}Br_2$ concentrations in Table 1. The time points when protofibrils or fibrils appear correspond well to the points when the solution turbidity starts to increase or reach equilibrium, respectively.

Amyloid fibrillogenesis is usually accepted as a two-step process that is an initial rate-limiting nucleation step followed by a rapid fibril elongation step.[3,32] Both hydrophobic interaction and electrostatic interaction play important roles in Aβ fibrillogenesis.[33,34] Hills, Jr. et al.[35] have demonstrated that the hydrophobic effect is the primary thermodynamic driving force in amyloid protein nucleation. Saiki et al.[36] reported the hydrophobic interaction between the respective paired side chains on the coupled β-strands were essential for fibril formation. Molecular dynamics simulations have also confirmed the important role of hydrophobic interactions in amyloid fibrillization.[37] Besides, Guo et al.[34] have demonstrated that repulsive electrostatic interactions impede the oligomerization of Aβ peptide.

The effect of $C_{12}C_6C_{12}Br_2$ concentration on Aβ(1−40) fibrillogenesis rate may also be ascribed to its influence on the hydrophobic/electrostatic balance in the system. Surfactant molecules might interfere with the amyloid aggregation by mainly affecting the nuclei formation.[24] In the case of 0.05 mM $C_{12}C_6C_{12}Br_2$, the positive charges of surfactant are comparable with the negative charges of Aβ(1−40) in number. $C_{12}C_6C_{12}Br_2$ monomers bind onto Aβ(1−40) molecules through electrostatic attraction, neutralizing Aβ(1−40) and exposing the surfactant hydrophobic tails to the medium. This greatly reduces the solubility of the Aβ/surfactant complexes. Simultaneously, the intra- and/or intermolecular hydrophobic interactions increase greatly, which makes the folding of Aβ(1−40) molecules to form nuclei energetically favorable. These factors will result in the rapid nucleation and fibrillogenesis of Aβ(1−40). However, in the case of 0.3 mM $C_{12}C_6C_{12}Br_2$, the surfactant positive charges are in excess of the Aβ negative charges. The excess $C_{12}C_6C_{12}Br_2$ molecules would further bind onto the Aβ/surfactant complexes through hydrophobic interaction to form surfactant clusters. These surfactant clusters expose a certain amount of positive charges outward and introduce electrostatic repulsion into the complexes, which raises the nucleation energy barrier and accordingly reduces the Aβ fibrillogenesis rate. Then, in the case of 2.5 mM $C_{12}C_6C_{12}Br_2$, the binding of surfactant micelles on Aβ(1−40) inhibits the nucleation by greatly enhancing both electrostatic repulsion and steric hindrance. In this case, the folding of Aβ(1−40) molecules is energetically unfavorable. Thus, both the nucleation and fibrillogenesis rates decrease greatly.

Effect of Gemini Surfactant on Size and Morphology of Aβ(1−40) Aggregates. $C_{12}C_6C_{12}Br_2$ can affect not only the fibrillogeneis rate of Aβ(1−40) but also the size and morphology of the aggregates. The following text will discuss the size and morphology of the Aβ(1−40) aggregates at different assembly stages.

Oligomers. Figure 2 shows the morphologies of the early-stage Aβ(1−40) aggregates formed at different $C_{12}C_6C_{12}Br_2$ concentrations. The spherical aggregates should be the oligomers, present in all these images. However, there are some aggregates with either a large size or irregular shape in the presence of 0.3 and 2.5 mM $C_{12}C_6C_{12}Br_2$. These aggregates may be categorized as the amorphous aggregates, as will be discussed in a later section. The distribution of the oligomer diameters in each case is listed in Table 2. Measurements of the height rather than the width are used as estimates of the diameters of Aβ aggregate species due to the AFM tip-related convolution effect.[32,38] In each case, at least 200 individual aggregates from different sample areas were analyzed. The reported values are averages of these measurements. As seen from Table 2, for the oligomers formed by Aβ(1−40) itself, most of them (∼85%) are in the size range of <4.0 nm, and only a very small portion (∼13%) of oligomers show larger diameters of 4.0−8.0 nm. However, with increasing $C_{12}C_6C_{12}Br_2$ concentration, the number of smaller oligomers decreases while the number of larger oligomers increases. In the cases of 0.3 and 2.5 mM $C_{12}C_6C_{12}Br_2$, some oligomers with even larger size (>8.0 nm) appear.

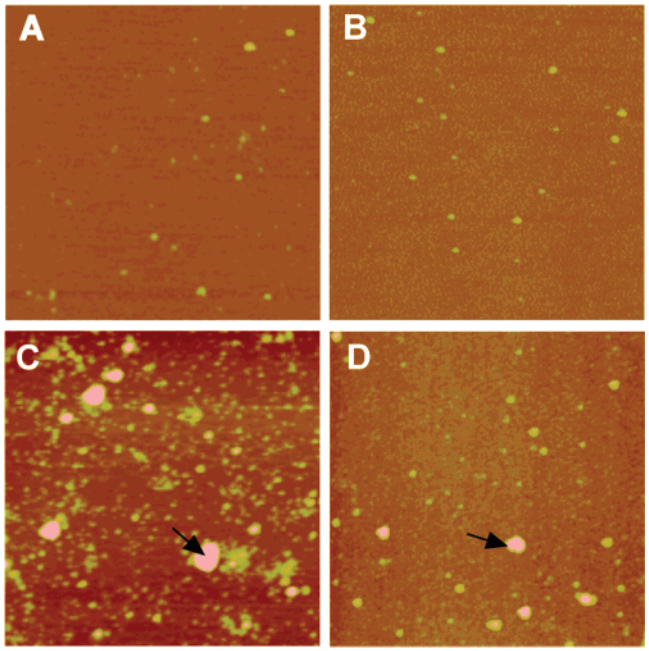

Figure 2. Morphologies of the oligomers formed (A) in the absence of $C_{12}C_6C_{12}Br_2$ or in the presence of (B) 0.05, (C) 0.3, and (D) 2.5 mM $C_{12}C_6C_{12}Br_2$. All the images are 2.5 × 2.5 μm^2 in size.

TABLE 2: Distribution (%) of the Oligomer Diameters at Different $C_{12}C_6C_{12}Br_2$ Concentrations

concentrations	<4.0 nm	4.0−8.0 nm	>8.0 nm
0 mM $C_{12}C_6C_{12}Br_2$	85	13	2
0.05 mM $C_{12}C_6C_{12}Br_2$	65	32	3
0.3 mM $C_{12}C_6C_{12}Br_2$	47	38	15
2.5 mM $C_{12}C_6C_{12}Br_2$	24	50	26

Two aspects may influence the oligomer sizes. One is the binding of $C_{12}C_6C_{12}Br_2$ molecules with the oligomers, and the other is the change in the assembling style of $A\beta(1-40)$ molecules caused by its interaction with the surfactant. However, we cannot differentiate these two aspects from the AFM images.

Protofibrils. Figure 3 presents the morphologies of $A\beta(1-40)$ protofibrils assembled at different surfactant concentration. The protofibrils assembled in different cases show great distinction in number, size, and morphology. In the absence of $C_{12}C_6C_{12}Br_2$ and in the presence of 0.05 mM $C_{12}C_6C_{12}Br_2$, the $A\beta(1-40)$ protofibrils have a morphology transition from the early-stage protofibrils (images A(a) and B(a)) to the lateral-packed (image A(b)) or interconnected (image B(b)) protofibrils. The lengths of the protofibrils also change from nanometer scale to submicrometer scale during the process. However, in the presence of 0.3 and 2.5 mM $C_{12}C_6C_{12}Br_2$, the protofibrils tend to be irregular in shape and always show a rough surface. The protofibrils show no lateral-packing or interconnecting during this stage.

Fibrils. Figure 4 presents the morphologies of $A\beta(1-40)$ fibrils assembled at different $C_{12}C_6C_{12}Br_2$ concentrations. The fibrils show great differences in their packing styles among different cases. In the absence of $C_{12}C_6C_{12}Br_2$, the fibrils tend to form parallel-aligned fibril assembly through lateral association (Figure $4A_2$ and $4A_3$). In the presence of 0.05 mM $C_{12}C_6C_{12}Br_2$, the fibrils show a higher tendency to pack together and form large fibril bundles (Figure $4B_2$ and $4B_3$). This result indicates that the propensity for lateral association between fibrils is highly improved by the presence of 0.05 mM $C_{12}C_6C_{12}Br_2$. However, unlike the case without $C_{12}C_6C_{12}Br_2$, the lateral association here causes the formation of randomly packed fibril bundles with irregular morphologies rather than the parallel-aligned fibril assembly. Then, at 0.3 and 2.5 mM $C_{12}C_6C_{12}Br_2$, a common striking feature is that the fibrils spread apart (Figure 4C, D). It seems that the lateral association between the fibrils is weakened or even totally inhibited. In summary, both AFM images and TEM images reveal that amyloid fibrils are extremely diverse in morphology, especially in the absence of $C_{12}C_6C_{12}Br_2$ and in the presence of 0.05 mM $C_{12}C_6C_{12}Br_2$.

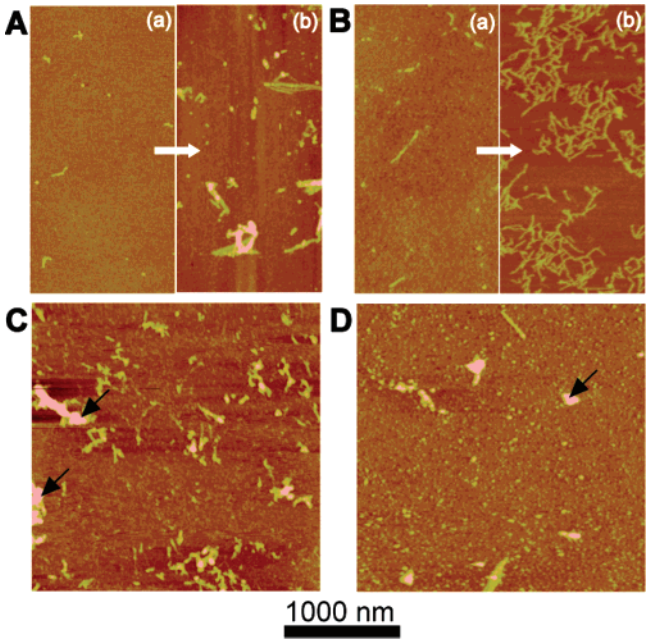

Figure 3. Morphologies of $A\beta(1-40)$ protofibrils assembled (A) in the absence of $C_{12}C_6C_{12}Br_2$ or in the presence of (B) 0.05 mM, (C) 0.3 mM, and (D) 2.5 mM $C_{12}C_6C_{12}Br_2$.

Table 3 presents the distribution of the fibril diameters at different size range at different surfactant cncentrations. The fibril diameter distribution shows complicated changes with increasing $C_{12}C_6C_{12}Br_2$ concentration. For $A\beta(1-40)$ itself, the number of fibrils with small diameters of <4.0 nm is comparable to that with the diameters of 4.0−8.0 nm. Approximately 13% of the fibrils show diameters larger than 8.0 nm. At 0.05 mM $C_{12}C_6C_{12}Br_2$, the fraction of the fibrils with larger diameters increases, while that with smaller diameters decreases greatly. Then, at 0.3 mM $C_{12}C_6C_{12}Br_2$, most of the fibrils (~96%) show diameters smaller than 8.0 nm. The fraction of fibrils with large diameters decreases sharply to only 4%. At last, at 2.5 mM $C_{12}C_6C_{12}Br_2$, most of the fibrils (~80%) have diameters of 4.0−8.0 nm.

To gain insight into the fine structures of the amyloid fibrils, we present the high-magnification morphology images in Figure 5. The broad morphological diversity in fibrils, with respect to their width, height, and twisting patterns, is seen clearly from these images. In the absence of $C_{12}C_6C_{12}Br_2$ (Figure 5, parts A_1-A_5), one most prominent fibrillar type seems to be the straight or slightly curvy, rod-shaped fibrils (white arrows) with the height of 2.8 ± 0.5 nm. This type of fibrils seems to be in lower-order and many other types of higher-order fibrils are produced through their lateral association, such as the ribbon-like fibrils (white arrow heads) and the twisted fibrils (black arrow heads). This lower-order to higher-order transition of fibrillar types can be clearly seen from the splitting of some ribbon-like fibrils and twisted fibrils into two or more rod-shaped fibrils. The twisted fibril displays an irregular twisting pattern, which seems to be able to switch even within individual fibrils. One typical twisted fibril with the diameter of ~6.5 nm is shown

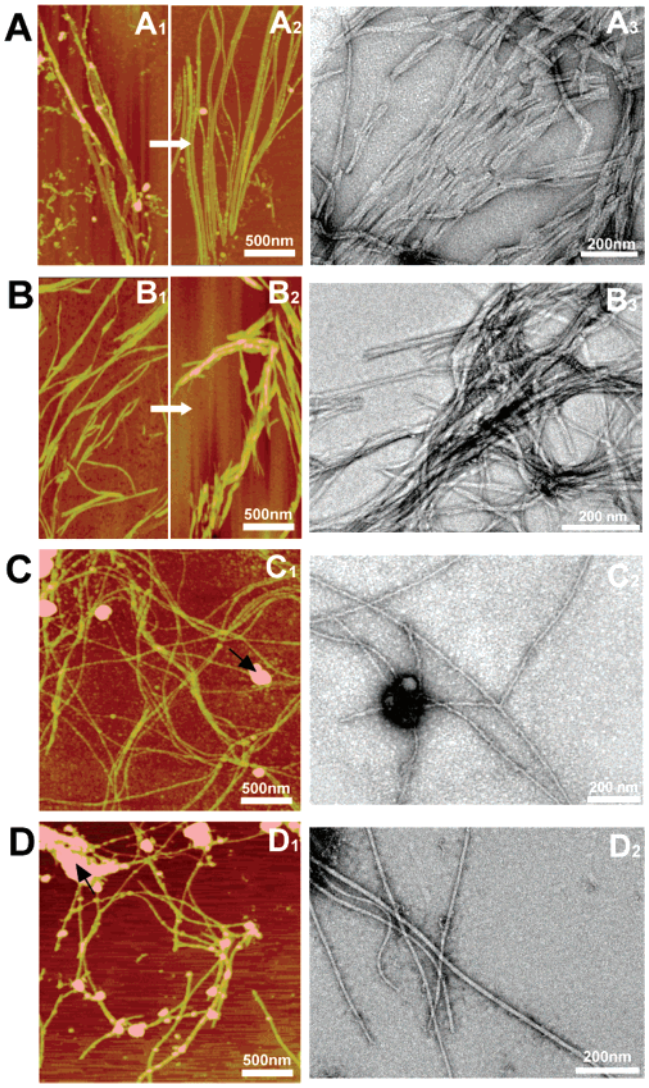

Figure 4. Morphologies of Aβ(1−40) fibrils assembled (A) in the absence of $C_{12}C_6C_{12}Br_2$ or in the presence of (B) 0.05 mM, (C) 0.3 mM, and (D) 2.5 mM $C_{12}C_6C_{12}Br_2$. Left: AFM height images; right: TEM images.

TABLE 3: Distribution (%) of the Fibril Diameters at Different $C_{12}C_6C_{12}Br_2$ Concentrations

concentrations	<4.0 nm	4.0−8.0 nm	>8.0 nm
0 mM $C_{12}C_6C_{12}Br_2$	45	42	13
0.05 mM $C_{12}C_6C_{12}Br_2$	15	66	19
0.3 mM $C_{12}C_6C_{12}Br_2$	38	58	4
2.5 mM $C_{12}C_6C_{12}Br_2$	14	80	6

in Figure 5A$_3$. Its smallest twisting periodicity is 28 nm while the largest one reaches 57 nm. Similar results of aperiodic twisting in amyloid fibrils have also been reported by Goldsbury et al.,[11] Anderson et al.,[38] and some other groups. The ribbon-like fibril also shows a variation in the number of constitutive protofibrils at its different parts, as seen from the fibril indicated by the white arrowhead in Figure 5A$_5$. Moreover, most of the fibrils show smooth surfaces except for some oscillations in height caused by oligomer attaching.

Formation of the different types of fibrils, including rod-like fibrils, twisted fibrils, and ribbon-like fibrils that vary in both diameters and morphologies, suggests that not only the number of lower-order fibrils that comprise the higher-order fibrils but also the manner in which the lower-order fibrils are assembled vary from fibril to fibril,[39] that is, several alternative modes of lateral association may coexist under the same growth condition.

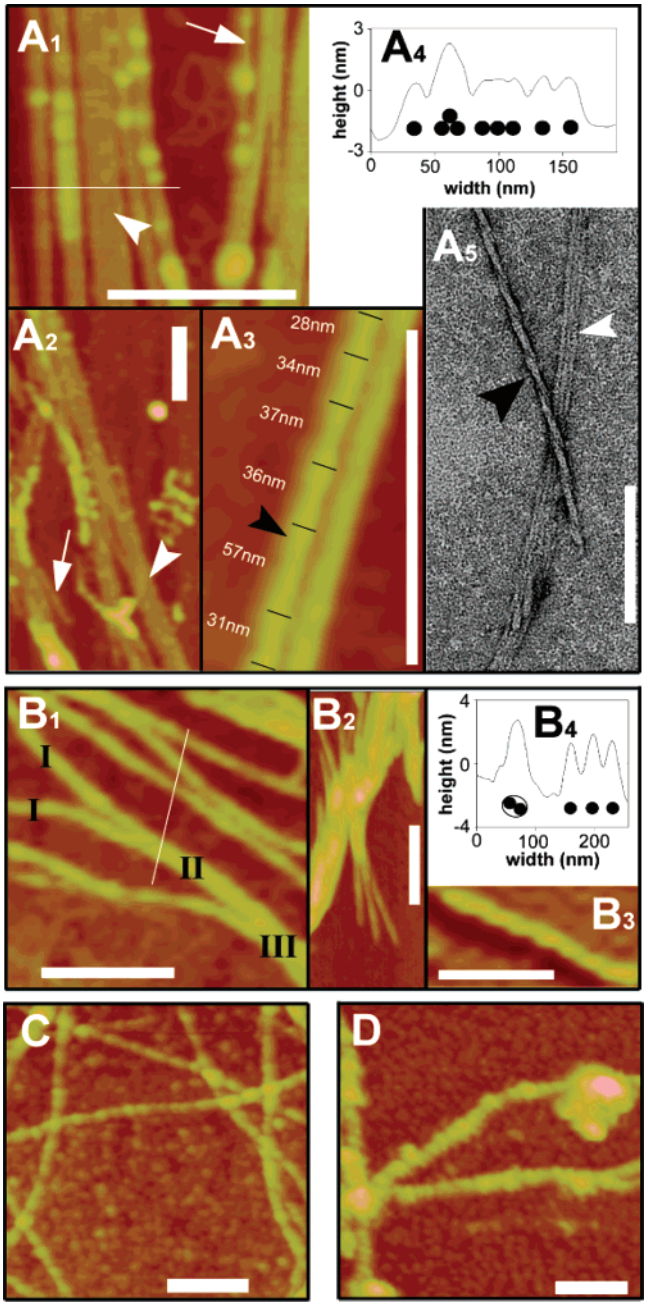

Figure 5. The fine structures of Aβ(1−40) fibrils assembled (A$_1$−A$_5$) in the absence of $C_{12}C_6C_{12}Br_2$ or in the presence of (B$_1$−B$_4$) 0.05 mM, (C) 0.3 mM, and (D) 2.5 mM $C_{12}C_6C_{12}Br_2$. Scale bars represent 200 nm in all the images.

In Figure 5A$_4$, several probable packing manners of the lower-order fibrils are drawn under the corresponding section analysis.

The fibrils formed at 0.05 mM $C_{12}C_6C_{12}Br_2$ (Figure 5 B$_1$−B$_4$) also show a variety of morphologies including rod-shaped fibrils (Figure 5B$_1$), rod bundles (Figure 5B$_2$), and twisted fibrils (Figure 5B$_3$). In Figure 5B$_1$, we label out several types of fibrils that are in different number levels. Among them, type I fibrils seem to be in the lower-order, while fibrils II and III are formed by type I fibrils of 2 and 3, respectively, clearly seen from the splitting of the fibrils. The possible packing manners of the lower-order fibrils in different fibril types are indicated under the corresponding section analysis (Figure 5B$_4$).

Then, in the cases of 0.3 (Figure 5C) and 2.5 mM (Figure 5D) $C_{12}C_6C_{12}Br_2$, no prominent morphological diversity can be found and the fibrils show new features in morphology. At 0.3 mM $C_{12}C_6C_{12}Br_2$, most of the fibrils show a beaded nature.

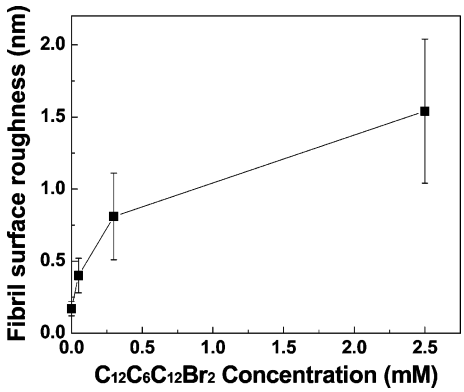

Figure 6. The surface roughness of the Aβ(1−40) fibrils formed at different $C_{12}C_6C_{12}Br_2$ concentrations. In each case, at least 50 individual fibrils from different samples were analyzed at different parts.

These fibrils show variable oscillations in height along the fibril axis. At 2.5 mM $C_{12}C_6C_{12}Br_2$, most of the fibrils exhibit rough surfaces and show a variation in diameter.

Figure 6 presents the surface roughness values of the Aβ-(1−40) fibrils formed at different $C_{12}C_6C_{12}Br_2$ concentrations. As seen, the fibril surface roughness increases with increasing $C_{12}C_6C_{12}Br_2$ concentration. This result indicates that with more and more surfactant molecules bound onto Aβ(1−40), the surface of the fibrils become more uneven.

Amorphous Aggregates. In the presence of 0.3 and 2.5 mM $C_{12}C_6C_{12}Br_2$, besides the typical Aβ aggregates of oligomers, protofibrils, and fibrils, one special aggregate form—amorphous aggregates—appears and is present during the whole fibrillogenesis process, as indicated by the black arrows in the AFM images of Figures 2−4. These aggregates are usually irregular in morphology and larger in size (10−50 nm in height). This result indicates that $C_{12}C_6C_{12}Br_2$ may induce another aggregation pathway for Aβ peptide by altering the folding style of the peptide. As demonstrated by Lorenzo et al.,[14] these amorphous aggregates might have no neurotoxicity.

$C_{12}C_6C_{12}Br_2$ may affect the morphologies and sizes of Aβ-(1−40) aggregates through binding on Aβ(1−40) and, in turn, alter its aggregation pathway. For all the aggregates assembled in different fibrillogenesis stages, binding of $C_{12}C_6C_{12}Br_2$ molecules on Aβ(1−40) may enlarge the aggregate size, broaden their size distribution, and affect their surface roughness. Appearance of amorphous aggregates at both 0.3 and 2.5 mM $C_{12}C_6C_{12}Br_2$ should be produced via altering the Aβ(1−40) aggregation pathway.

During the fibril formation, certain amino acid side chains are exposed on the fibrils surface, which can greatly alter the surface properties of the fibrils and influence fibril−fibril interactions.[10,40] Previous study by Marek et al.[41] revealed that aromatic interactions, including both aromatic π-stacking and aromatic hydrophobic interaction, could influence the fibril morphology of islet amyloid polypeptide by mediating interfibril interactions and subsequent fibril hierarchical assembly.

$C_{12}C_6C_{12}Br_2$ may influence the lateral association by adjusting the balance of electrostatic/hydrophobic interactions between the fibrils. For Aβ(1−40) itself, $\pi-\pi$ stacking between aromatic groups on the fibril surface may be one of the dominant driving forces for interfibril packing. The aromatic $\pi-\pi$ stacking is specific in its site-recognizing property. Reasonably, it will result in relatively regular packing of the lower-order fibrils. However, at 0.05 mM $C_{12}C_6C_{12}Br_2$, the surfactant monomers bind on Aβ-(1−40) electrostatically and expose their hydrocarbon chains to the medium. This enhances the number of hydrophobic groups

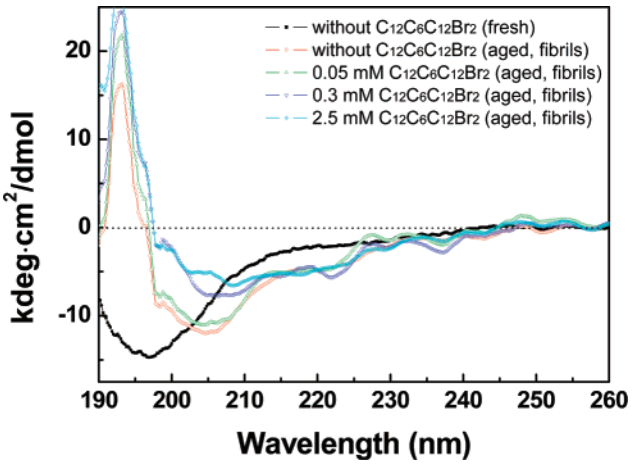

Figure 7. CD spectra of the amyloid solutions in the absence of $C_{12}C_6C_{12}Br_2$ and in the presence of different concentrations of $C_{12}C_6C_{12}Br_2$.

TABLE 4: Fractions of Various Secondary Structures in the Aged Aβ Solutions

concentrations	α-helix	β-sheet	random coils
0 mM $C_{12}C_6C_{12}Br_2$	0.07	0.50	0.43
0.05 mM $C_{12}C_6C_{12}Br_2$	0.07	0.51	0.42
0.3 mM $C_{12}C_6C_{12}Br_2$	0.13	0.33	0.54
2.5 mM $C_{12}C_6C_{12}Br_2$	0.17	0.30	0.53

on the fibril surface, and thus it greatly strengthens the hydrophobic interaction between fibrils and elevates the propensity for lateral association. However, unlike specific aromatic $\pi-\pi$ stacking, the hydrophobic interaction between hydrocarbon chains is nonspecific in nature and therefore results in the random packing of the fibrils to form irregular fibril bundles. For 0.3 and 2.5 mM $C_{12}C_6C_{12}Br_2$, the same charged surfactant aggregates on the fibril surface and introduces electrostatic repulsion between fibrils. This factor makes it unfavorable for fibrils to pack together, and thus the lateral association between fibrils is weakened or cannot be underway at all.

The change in lateral association upon increasing $C_{12}C_6C_{12}Br_2$ concentration affects the formation of the higher-order fibrils through the assembly of the lower-order fibrils. It then changes the morphological diversity in fibrils. This effect, together with the binding of $C_{12}C_6C_{12}Br_2$ molecules, finally causes the variation of the distribution of the fibril diameters with $C_{12}C_6C_{12}Br_2$ concentration.

Effect of Gemini Surfactant on the Secondary Structure of Aged Aβ(1−40). In order to inquire into the possible secondary structural changes due to the influence of $C_{12}C_6C_{12}Br_2$ concentrations, we carried out CD measurements. The results are shown in Figure 7. As seen, the spectrum of the fresh native Aβ(1−40) is characterized by a minimum at 197 nm, reflecting the predominant random-coil structure of the peptide.[42] However, the spectra of aged Aβ(1−40) solutions all present broad negative bands in the wavelength range 205−222 nm, which indicates a rearrangement of the peptide structure into a conformation rich in α-helix and/or β-sheets. Table 4 gives the percentages of each secondary structure in the amyloid aggregates analyzed using the K2D program. The fraction of turns is included in the percentage of random coils in this analysis method. The K2D calculations show that the content of each secondary structure varies with the $C_{12}C_6C_{12}Br_2$ concentration. Without $C_{12}C_6C_{12}Br_2$ or in the presence of 0.05 mM $C_{12}C_6C_{12}Br_2$, the secondary structure contents are similar, which are about 7% α-helix, 50% β-sheets, and the rest for random coils. However, upon increasing $C_{12}C_6C_{12}Br_2$ concentration to 0.3 and

2.5 mM, the contents of both α-helix and random coils increase, but β-sheet conformation decreases dramatically. Since the positive charges of $C_{12}C_6C_{12}Br_2$ are in excess of the negative charges of Aβ(1−40) in these two cases, the CD results here indicate that the excess positive charges seem to be able to stabilize the structure of α-helix and random coils while inhibit β-sheet formation. Both the increased electrostatic repulsion in the system and the interaction between residues Phe19 and Phe20 of Aβ(1−40) and the surfactant hydrophobic chains may be important in preventing this α-helix to β-sheet transformation.[43] In the study of the Aβ(1−28)/DPC system, Ma et al.[43] have proposed the possibility of this interaction from NMR results. However, no direct experimental evidence has been obtained currently.

From the above results, we can see that the electrostatic/hydrophobic force balance in the system plays important roles in determining the aggregation pathways, the size and morphology of the aggregates, and the secondary structures of Aβ(1−40). The molecular modeling may help to understand the electrostatic/hydrophobic force balance and the binding of surfactant with the peptide. However, to our knowledge, so far the calculations mainly focus on modeling the Aβ molecule itself.[35,37] Involving surfactant molecules in the modeling makes the calculation more complicated and difficult to carry out. As inferred from the present experimental results, the effects of hydrophobic/electrostatic interactions on the size and morphology of the aggregates are more likely to be kinetically controlled. In the present study, the incubation time is probably not sufficient for the system to reach thermodynamic equilibrium. The size and morphology of the aggregates show strong dependence on time. With the elapse of time, the aggregates show evolution in the order of monomers, oligomers, protofibrils, and fibrils. These different aggregates are probably caused by competition between different aggregation pathways and competition between different lateral association modes of lower-order fibrils. If the kinetic barrier for one pathway is lower than that for another one, this pathway will proceed and produce the corresponding aggregate form.

Conclusions

The present work studies the effect of the surfactant concentration on the dynamics of Aβ fibrillogenesis, and the morphologies, sizes, and the secondary structures of Aβ aggregates with time. The results show that the cationic gemini surfactant $C_{12}C_6C_{12}Br_2$ can regulate the fibrillogenesis of Aβ(1−40) peptide. Modulation of the electrostatic interaction and the hydrophobic interaction in the system can affect not only the nucleation of Aβ(1−40), but also its secondary structures and the lateral association between the fibrils. At low $C_{12}C_6C_{12}Br_2$ monomer concentration where the surfactant positive charges are close to the Aβ(1−40) negative charges in number, hydrophobic interaction is highly enhanced in the system. Hence, both the Aβ(1−40) nucleation rate and the lateral association between fibrils are greatly promoted. While for higher $C_{12}C_6C_{12}Br_2$ monomer concentration or $C_{12}C_6C_{12}Br_2$ micelles where the surfactant positive charges are in excess of the Aβ(1−40) negative charges, electrostatic repulsion is strengthened. In this case, the nucleation rate is decreased, the lateral association is inhibited, and the α-helix to β-sheet secondary structural transition is prevented. Simultaneously, another assembly pathway is induced to give the amorphous aggregates. Moreover, the binding of the $C_{12}C_6C_{12}Br_2$ molecules onto Aβ(1−40) can also affect the size and surface roughness of the aggregates. These findings of our work may be helpful in guiding the development and design of an effective reagent to control the aggregation of Aβ(1−40) for AD therapy.

Acknowledgment. We are grateful for financial support from the National Science Foundation of China (20633010, 20573123).

Supporting Information Available: Series of AFM height images showing the fibrillogenesis of Aβ(1−40) on time in the absence of $C_{12}C_6C_{12}Br_2$ or in the presence of different concentrations of $C_{12}C_6C_{12}Br_2$. This material is available free of charge via the Internet at http://pubs.acs.org.

References and Notes

(1) (a) Cohen, A. S.; Calkins, E. *Nature* **1959**, *183*, 1202−1203. (b) Selkoe, D. J. *Science* **1997**, *275*, 630−631.

(2) Hardy, J.; Selkoe, D. J. *Science* **2002**, *297*, 353−356.

(3) Clippingdale, A. B.; Wade, J. D.; Barrow, C. J. *J. Pept. Sci*. **2001**, *7*, 227−249.

(4) (a) Barrow, C. J.; Zagorski, M. G. *Science* **1991**, *253*, 179−182. (b) Burdick, D.; Soreghan, B.; Kwon, M.; Kosmoski, J.; Knauer, M.; Henschen, A.; Yates, J.; Cotman, C.; Glabe, C. *J. Biol. Chem.* **1992**, *267*, 546−554.

(5) (a) Snyder, S. W.; Ladror, U. S.; Wade, W. S.; Wang, G. T.; Barrett, L. W.; Matayoshi, E. D.; Huffaker, H. J.; Krafft, G. A.; Holzman, T. F. *Biophys. J.* **1994**, *67*, 1216−1228. (b) Sabaté, R.; Estelrich, J. *J. Phys. Chem. B* **2005**, *109*, 11027−11032. (c) Halverson, K.; Fraser, P. E.; Kirschner, D. A.; Lansbury, P. T. *Biochemistry* **1990**, *29*, 2639−2644. (d) Harper, J. D.; Wong, S. S.; Lieber, C. M.; Lansbury, P. T., Jr. *Biochemistry* **1999**, *38*, 8972−8980. (e) Nichols, M. R.; Moss, M. A.; Reed, D. K.; Lin, W.-L.; Mukhopadhyay, R.; Hoh, J. H.; Rosenberry, T. L. *Biochemistry* **2002**, *41*, 6115−6127. (f) Lovell, M. A.; Robertson, J. D.; Teesdale, W. J.; Campbell, J. L.; Markesbery, W. R. *J. Neurol. Sci*. **1998**, *158*, 47−52.

(6) (a) Bush, A. I.; Pettingell, W. H.; Multhaup, G.; Paradis, M. D.; Vonsattel, J.-P.; Gusella, J. F.; Beyreuther, K.; Masters, C. L.; Tanzi, R. E. *Science* **1994**, *265*, 1464−1467. (b) McAllister, C.; Karymov, M. A.; Kawano, Y.; Lushnikov, A. Y.; Mikheikin, A.; Uversky, V. N.; Lyubchenko, Y. L. *J. Mol. Biol*. **2005**, *354*, 1028−1042.

(7) Lomakin, A.; Chung, D. S.; Benedek, G. B.; Kirschner, D. A.; Teplow, D. B. *Proc. Natl. Acad. Sci. U.S.A.* **1996**, *93*, 1125−1129.

(8) (a) Serpell, L. C. *Biochim. Biophys. Acta* **2000**, *1502*, 16−30. (b) Antzuktin, O. N.; Leapman, R. D.; Balbach, J. J.; Tycko, R. *Biochemistry* **2002**, *41*, 15436−15450.

(9) Nichols, M. R.; Moss, M. A.; Reed, D. K.; Cratic-McDaniel, S.; Hoh, J. H.; Rosenberry, T. L. *J. Biol. Chem.* **2005**, *280*, 2471−2480.

(10) Petkova, A. T.; Leapman, R. D.; Guo, Z. H.; Yau, W.-M.; Mattson, M. P.; Tycko, R. *Science* **2005**, *307*, 262−265.

(11) Goldsbury, C.; Frey, P.; Olivieri, V.; Aebi, U.; Müller, S. A. *J. Mol. Biol.* **2005**, *352*, 282−298.

(12) Lührs, T.; Ritter, C.; Adrian, M.; Riek-Loher, D.; Bohrmann, B.; Döbeli, H.; Schubert, D.; Riek, R. *Proc. Natl. Acad. Sci. U.S.A.* **2005**, *102*, 17342−17347.

(13) Seilheimer, B.; Bohrmann, B.; Bondolfi, L.; Muller, F.; Stuber, D.; Dobeli, H. *J. Struct. Biol.* **1997**, *119*, 59−71.

(14) Lorenzo, A.; Yankner, B. A. *Proc. Natl. Acad. Sci. U.S.A.* **1994**, *91*, 12243−12247.

(15) Kremer, J. J.; Pallitto, M. M.; Sklansky, D. J.; Murphy, R. M. *Biochemistry* **2000**, *39*, 10309−10318.

(16) Walsh, D. M.; Klyubin, I.; Fadeeva, J. V.; Cullen, W. K.; Anwyl, R.; Wolfe, M. S.; Rowan, M. J.; Selkoe, D. J. *Nature* **2002**, *416*, 535−539.

(17) Cohen, E.; Bieschke, J.; Perciavalle, R. M.; Kelly, J. W.; Dillin, A. *Science* **2006**, *313*, 1604−1610.

(18) Kessler, J. C.; Rochet, J.-C.; Lansbury, P. T., Jr. *Biochemistry* **2003**, *42*, 672−678.

(19) (a) Nowick, J. S.; Lam, K. S.; Khasanova, T.; Kemnitzer, W. E.; Maitra, S.; Mee, H. T.; Liu, R. *J. Am. Chem. Soc*. **2002**, *124*, 4972−4973. (b) Lowe, T.; Strzelec, A.; Kiessling, L. L.; Murphy, R. M. *Biochemistry* **2001**, *40*, 7882−7889. (c) Pallitto, M.; Murphy, R.; Ghanta, J.; Heinzelman, P.; Kiessling, L. L. *Biochemistry* **1999**, *38*, 3570−3578. (d) Ban, T.; Hoshino, M.; Takahashi, S.; Hamada, D.; Hasegawa, K.; Naiki, H.; Goto, Y. *J. Mol. Biol*. **2004**, *344*, 757−767.

(20) Pertinhez, T. A.; Bouchard, M.; Smith, R. A. G.; Dobson, C. M.; Smith, L. J. *FEBS Lett.* **2002**, *529*, 193−197.

(21) Shao, H.; Jao, S.-C.; Ma, K.; Zagorski, M. G. *J. Mol. Biol.* **1999**, *285*, 755−773.

(22) Wood, S. J.; MacKenzie, L.; Maleef, B.; Hurle, M. R.; Wetzel, R. *J. Biol. Chem.* **1996**, *271*, 4086−4092.

(23) Sabaté, R.; Estelrich, J. *Langmuir* **2005**, *21*, 6944−6949.

(24) Sabaté, R.; Gallardo, M.; Estelrich, J. *Biopolymers* **2003**, *71*, 190−195.

(25) Wang, S. S.-S.; Chen, Y.-T.; Chou, S.-W. *Biochim. Biophys. Acta* **2005**, *1741*, 307−313.

(26) Li, Y. J.; Cao, M. W.; Wang, Y. L. *J. Phys. Chem. B* **2006**, *110*, 18040−18045.

(27) (a) Menger, F. M.; Littau, C. A. *J. Am. Chem. Soc.* **1993**, *115*, 10083−10090. (b) Zana, R.; Benrraou, M.; Rueff, R. *Langmuir* **1991**, *7*, 1072−1075.

(28) Wood, S. J.; Maleeff, B.; Hart, T.; Wetzel, R. *J. Mol. Biol.* **1996**, *256*, 870−877.

(29) (a) Lobley, A.; Whitmore, L.; Wallace, B. A. *Bioinformatics* **2002**, *18*, 211−212. (b) Whitmore, L.; Wallace, B. A. *Nucleic Acids Res.* **2004**, *32*, W668−W673.

(30) Harper, J. D.; Wong, S. S.; Lieber, C. M.; Lansbury, P. T., Jr. *Chem. Biol.* **1997**, *4*, 119−125.

(31) (a) Alami, E.; Beinert, G.; Marie, P.; Zana, R. *Langmuir* **1993**, *9*, 1465−1467. (b) Wang, X.; Li, Y.; Wang, J.; Wang, Y.; Ye, J.; Yan, H.; Zhang, J.; Thomas, R. K. *J. Phys. Chem. B* **2005**, *109*, 12850−12855.

(32) Wetzel, R. *Amyloid, Prions, and other Protein Aggregates*; Academic Press: San Diego, 1999.

(33) (a) Ghanta, J.; Shen, C.-L.; Kiessling, L. L.; Murphy, R. M. *J. Biol. Chem.* **1996**, *271*, 29525−29528. (b) Lansbury, P. T., Jr. *Acc. Chem. Res.* **1996**, *29*, 317−321. (c) Tycko, R. *Biochemistry* **2003**, *42*, 3151−3159.

(34) Guo, M.; Gorman, P. M.; Rico, M.; Chakrabartty, A.; Laurents, D. V. *FEBS Lett.* **2005**, *579*, 3574−3578.

(35) Hills, R. D., Jr.; Brooks, C. L., III. *J. Mol. Biol.* **2007**, *368*, 894−901.

(36) Saiki, M.; Honda, S.; Kawasaki, K.; Zhou, D. S.; Kaito, A.; Konakahara, T.; Morii, H. *J. Mol. Biol.* **2005**, *348*, 983−998.

(37) Nguyen, H. D.; Hall, C. K. *Proc. Natl. Acad. Sci. U.S.A.* **2004**, *101*, 16180−16185.

(38) Anderson, M.; Bocharova, O. V.; Makarava, N.; Breydo, L.; Salnikov, V. V.; Baskakov, I. V. *J. Mol. Biol.* **2006**, *358*, 580−596.

(39) (a) Khurana, R.; Ionescu-Zanetti, C.; Pope, M.; Li, J.; Nielson, L.; Ramírez-Alvarado, M.; Regan, L.; Fink, A. L.; Carter, S. A. *Biophys. J.* **2003**, *85*, 1135−1144. (b) Kad, N. M.; Myers, S. L.; Smith, D. P.; Smith, D. A.; Radford, S. E.; Thomson, N. H. *J. Mol. Biol.* **2003**, *330*, 785−797. (c) Goldsbury, C. S.; Cooper, G. J. S.; Goldie, K. N.; Müller, S. A.; Saafi, E. L.; Gruijters, W. T. M.; Misur, M. P.; Engel, A.; Aebi, U.; Kistler, J. *J. Struct. Biol.* **1997**, *119*, 17−27.

(40) (a) Malinchik, S. B.; Inouye, H.; Szumowski, K. E.; Kirschner, D. A. *Biophys. J.* **1998**, *74*, 537−545. (b) Fraser, P. E.; Nguyen, J. T.; Inouye, H.; Surewicz, W. K.; Selkoe, D. J.; Podlisny, M. B.; Kirschner, D. A. *Biochemistry* **1992**, *31*, 10716−10723.

(41) Marek, P.; Abedini, A.; Song, B.; Kanungo, M.; Johnson, M. E.; Gupta, R.; Zaman, W.; Wong, S. S.; Raleigh, D. P. *Biochemistry* **2007**, *46*, 3255−3261.

(42) Kuroda, Y.; Maeda, Y.; Sawa, S.; Shibata, K.; Miyamoto, K.; Nakagawa, T. *J. Pept. Sci.* **2003**, *9*, 212−220.

(43) (a) Ma, K.; Clancy, E. L.; Zhang, Y. B.; Ray, D. G.; Wollenberg, K.; Zagorski, M. G. *J. Am. Chem. Soc.* **1999**, *121*, 8698−8706. (b) Marcinowski, K. J.; Shao, H.; Clancy, E. L.; Zagorski, M. G. *J. Am. Chem. Soc.* **1998**, *120*, 11082−11091.